Bulletin of the Geological Society of Malaysia, Volume 72, November 2021, pp. 101 - 111
DOI: https://doi.org/10.7186/bgsm72202108

Seismic attributes for enhancing structural and stratigraphic features: Application to N-Field, Malay Basin, Malaysia

Nur Shafiqah Shahman[1,2,*], Norazif Anuar[1,2], Mohamed Elsaadany[1,2], Deva Prasad Ghosh[1,2]

[1] Department of Geoscience, Universiti Teknologi PETRONAS (UTP), 32610 Seri Iskandar, Perak, Malaysia
[2] Centre of Excellence in Subsurface Seismic Imaging & Hydrocarbon Prediction (CSI), Universiti Teknologi PETRONAS (UTP), 32610 Seri Iskandar, Perak, Malaysia
* Corresponding author email address: nurshafiqah_hafish94@yahoo.com

Abstract: Over two decades, analysis of seismic attributes had been an integral part of seismic reflection interpretation. Seismic attributes are an influential assistance to seismic interpretation, delivering geoscientists with alternative images of structural (faults) and stratigraphic features (channels), which can be utilised as mechanisms to identify prospects, ascertain depositional environment and structural deformation history more rapidly even provide direct hydrocarbon indicators. The additional steps are obligatory to compute and interpret the attributes of faults and channels from seismic images, which are often sensitive to noise due to the characteristically computed as discontinuities of seismic reflections. Furthermore, on a conventional seismic profile or poor quality data, faults and channels are hard to visible. The current research review these geological structures through a case study of 3D seismic data from N-field in the viewpoint of Malay Basin. This study aimed to characterise the structure and stratigraphic features by using seismic attributes on the N-field below seismic resolution. Also, two different methods are proposed to improve seismic reflections, i.e., faults and channels that are hard to see on the conventional 3D data set. The first method, to detect faults in seismic data, which this paper employs the ant tracking attribute as a unique algorithm to be an advanced forwarding that introduces a new tool in the interpretation of fault. The effective implementation of ant tracking can be achieved when the output of other faults sensitive attributes are used as input data. In this work, the seismic data used are carefully conditioned using a signal. Chaos and variance that are sensitive to faults are applied to the seismic data set, and the output from these processes are used as input data that run the ant tracking attribute, which the faults were seen difficult to display on the raw seismic data. Meanwhile, for the second method, spectral decomposition was adopted to deliberate the way its method could be utilised to augment stratigraphic features (channels) of the N-field, where the channel is ultimately considered being one of the largest formations of the petroleum entrapment. The spectral decomposition analysis method is an alternative practice concentrated on processing S-transform that can offer better results. Spectral decomposition has been completed over the Pleistocene channels, and results propose that application of its methods directs to dependable implications. Respective channel in this area stands out more obviously within the specific frequency range. The thinner layer demonstrates higher amplitude reading at a higher frequency, and the thicker channel displays higher amplitude reading at a lower frequency. Implementation of spectral decomposition assists in deciding the channels that were placed within incised valleys and helps in recognising the orientation and the relative thickness of each channel. By doing this, the ant tracking attribute and spectral decomposition approach have generated the details of subsurface geologic features through attributes by obtaining enhanced reflections and channels and sharpened faults, respectively.

Keywords: Seismic attributes, faults, ant tracking, channels, spectral decomposition

INTRODUCTION

In oil and gas exploration, both faults (structural) and channel (sedimentary distribution) are crucial configurations for gas accumulation. Generally, faults are paramount to represent reservoir boundaries and its compartmentalisation, so do the reservoir connectivity and continuity. It is relevant to recognise the timeline of fault growth by timing relatively relationship, especially in term of structure growth. The focus area in this study is N-Field, and it is located in the central part of the Malay Basin. The central part of Malay Basin has been inverted during Middle to Late Miocene. It started as an elongated east to west ridge due to changing stress directions and became more circular and commonly the area is associated with gas accumulation (Liew, 1997). According to Ngah (2000), during Oligocene and Miocene, the faults predominantly run in east-west and northwest-southeast directions. Presence of gas chimney or gas cloud confirms that some of these structures have been breached, and can impact the residual volume of hydrocarbon and channel in the reservoir. Several areas with existing faults are not very well defined in seismic data. As a result, the area that has poor imaging has introduced high uncertainty in fault interpretation. As in exploration, the presence of structural features is paramount importance for hydrocarbon entrapment. Therefore, the aim of this paper is to plausible the structure and stratigraphic features by using seismic attributes on the N-field area below seismic resolution.

0126-6187; 2637-109X / Published by the Geological Society of Malaysia.

N-FIELD

The N-Field is located offshore Terengganu, approximately 200 km northeast of Kemaman Supply Base in a water depth of 65.0 m (Figure 1). The block area is a large (250 km^2), faulted asymmetric anticline (Petronas, n.d.). Growth of the N-Field structure can be documented from Mid to Late Miocene (Group D and E), with the majority of the structural growth occurring in the Late Miocene (Group D). Compartmentalism of N-field structure is defined by three major fault blocks, i.e., east, central, and west. North-south trending faults bound each fault block with vertical closure varying from 50 m in the western fault block, 90 m in the central fault block to 140 m of closure in the eastern fault block. The east and west fault blocks are simple high-side fault blocks, which are situated within the central graben where numerous gas leak conduits exist (Petronas, n.d.). The several existing faults are not very well recognised due to the presence of substantial shallow gas cloud. Thus, N-Field has poor imaging in its crestal part where the gas cloud is rampant that introduced high uncertainty in fault interpretation.

GEOLOGICAL BACKGROUND OF STUDY AREA

In Malaysia's offshores (i.e., Peninsular, Sabah and Sarawak), the oil and gas reservoir occurs in a sedimentary rift basin, which the Malay Basin represents one of the most extensive rift basins in Southeast Asia region. The Malay Basin is an asymmetric northwest-southeast to NNW-SSE trending Cenozoic sedimentary basin elongated about 500 km long and 200 km wide. The Malay Basin is one of the deepest continental (measured roughly total sediment thickness exceeds 13,000 m) extensional basins in the Southeast region (Ngah, 2000). According to Metcalfe (1988), the tectonic framework of the Southeast Asia region is briefly summarised as the response of several small lithospheric plates to the convergence of the major Pacific, Eurasia and Indo Australia lithospheric plates. The western part of the Pacific plate moved west-northwestward relative to the Eurasia plate while the Indian Ocean floor with Australia moved relatively northward. The resultant movements of the small plates within the zone of interaction between large plates were therefore complex. The movements led to the

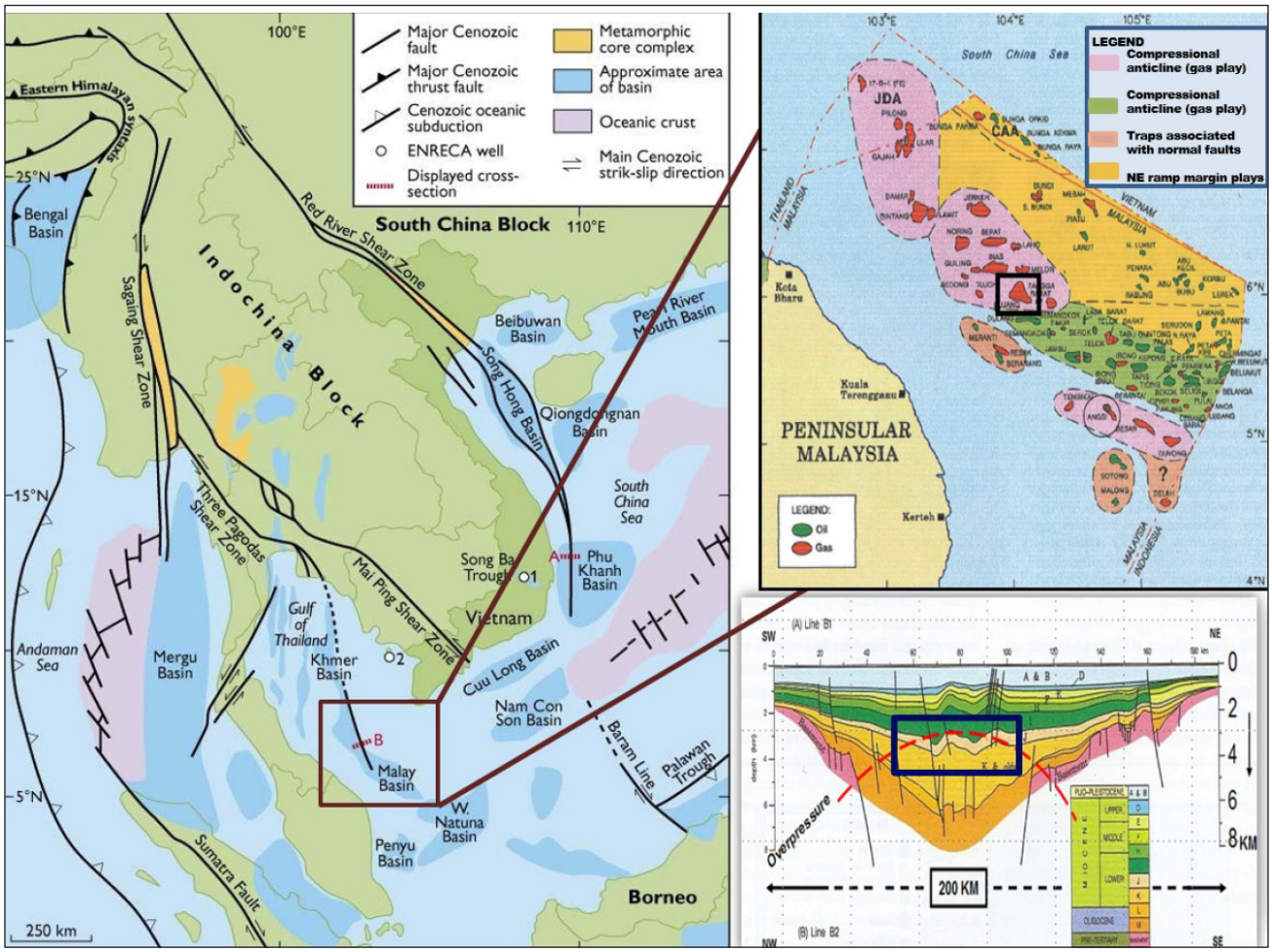

Figure 1: Location of the study area, N-Field (from Madon *et al.*, 1999), and structural cross-section of the Malay Basin, with 3D Seismic visualisation technique (from Ghosh *et al*., 2010).

formation of several small Tertiary basins, including the Malay Basin, that acted as receptacles for clastic sediment (Hutchison, 2014). The Malay Basin that started as an extensional rift basin by early Tertiary crustal extension and separated from the Pattani Basin in the north part by the Narathiwat High (Bishop, 2002) caused by strike-slip in nature along the major NW- SE trending shear zone. Malay Basin was built in three phases (Ngah, 2000):

1) Phase I: Late Cretaceous to Late Eocene (Extension phase)
2) Phase II: Late Miocene to Pliocene (Compression phase)
3) Phase III: Pliocene to Recent (Subsidence phase)

The N-Field structure was formed during phase I (extensional) and phase II (compressional) of the Malay Basin structure development. Referring to Madon *et al*. (1999), during Middle to Late Miocene, the structure of N-Field is alleged to form as a deep syncline within a half-graben. The altering stress direction causes the structure of N-Field started as an elongate east-west ridge and became more circular. The stratigraphy and depositional environment style can be documented from group F until early group B time.

STRATIGRAPHY AND DEPOSITIONAL ENVIRONMENT

As documented in Madon *et al*. (1999) and as shown in Figure 2, Group A's and B's sections are Plio-Miocene to recent in age. Group A's and B's sections are undifferentiated and overlie the Plio-Miocene unconformity, i.e., predominantly interbedded claystone and siltstone with minor sandstone. On the other hand, Group D's section is the Late Miocene in age and was deposited in a fluvial coastal plain environment and occurred immediately below the Plio-Miocene unconformity (made up of shale, siltstone with minor coal). Group E's section is the Late Miocene age, i.e., sand prone and interpreted to be fluvial and coastal plain deposits, predominantly made up of interbedded shale siltstone, sandstone and abundant coal. Meanwhile, Group F's section of Middle Miocene age is made up of interbedded shale with minor siltstone or sandstone. The lower section also has minor coal beds.

ATTRIBUTE ANALYSIS

Seismic attributes analysis is an excellent tool to obtain useful information to enhance or quantify features of interpretation that were not possible to detect on a seismic data set (Chopra & Marfurt, 2007a). The attributes allow the geoscientist to interpret structures (faults and fractures) and stratigraphic features (channels), recognise the depositional environment and explain the structural deformation promptly (Chopra & Marfurt, 2007b).

The methodology involved seismic interpretation and seismic attributes. Before the implementation of seismic attributes analysis, the seismic section needs to be interpreted structurally through a structural map. The seismic data is interpreted into seven seismic horizons based on different

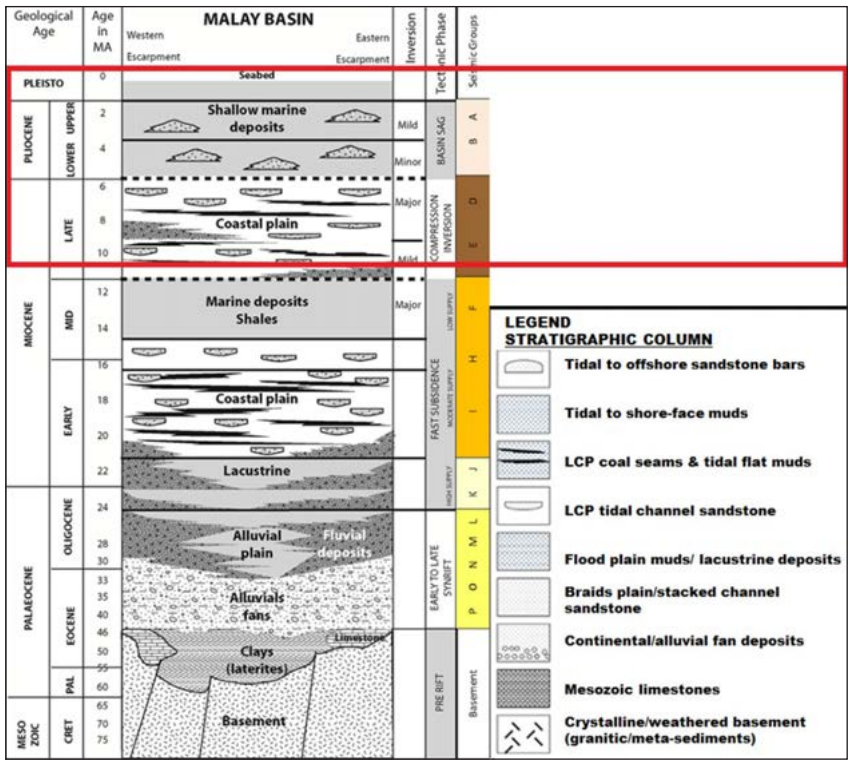

Figure 2: The stratigraphy column divided by group, environment, lithology, and structural events by time (from Mansor *et al*., 2014). The red box is the area of interest between Late Miocene to Recent.

depositional environments. A seismic interpretation was made using manual picking. For seismic attributes, the procedure involves ant tracking and spectral decomposition which will enable better imaging of discontinuities features. According to Ghosh *et al.* (2014), attributes categories are divided into three classes, i.e., Class 1 (structure attributes), Class 2 (spectral attributes), and Class 3 (fluid or lithology attributes). This paper applies the Class 1 and 2 for the identification of structural and geomorphological features.

Spectral decomposition

Spectral decomposition was conducted using Geomodelling software by Geomodeling Technology Corporation. The spectral decomposition method relies on 'tuning thickness' concept. According to Huang *et al.* (2016), spectral decomposition that extracted by seismic data need to decompose into time-frequency energy cubes when the time-dependent frequency response of subsurface rocks and reservoirs are going to be characterised. The composite reflection event equates the peak amplitude at ¼ wavelength of dominant bandwidth will respond at a different range of frequencies that help the channel features become conspicuous (Nanda, 2016). Alternatively, the tuning thickness of a thin bed will be scanned by the first spectral peak of the frequency simultaneously on the amplitude response showing maximum values (Nanda, 2016). The blue colour corresponds to a high frequency, while intermediate to low frequencies will be between red to green. The 3D seismic volume was superimposed on generating bodies that matched geological features using the RGB (red-green-blue) blending application. By combining RGB blending interpretation of volume cube, spectral decomposition will be converted into a single composite volume, in which RGB values are calculated by three basic frequencies, i.e. low, intermediate, and high frequencies. The thickest part of the channel appear in white, indicating that these parts have all the frequency range. The dark colour corresponds to low to middle frequency (i.e., orange and yellow) that also show low reflectivity. In this study, seismic data is converted into discrete frequency volumes and has been applied by S-transform algorithms in spectral decomposition. According to Martins *et al*. (2012), the S-transform algorithm create a time-frequency depiction of time series and is known for its local spectral phase tract (Kuyuk, 2015). The frequency-dependent resolution gives a unique combination simultaneously that is localised in between the real and the imaginary spectra. S-transform persists in ascribe phase information and has a frequency of constant amplitude response. On the other hand, it stands for the phase in the local spectrum setting and results in many advantaged characteristics (Stockwell, 2007).

Before applying the spectral decomposition, the frequency spectrum in the seismic data has to be identified. The result shows that the first and the second peak indicated in the frequency is 10 Hz and 50 Hz, respectively (Figure 3). Then, three frequencies were chosen, i.e., representing low frequency (10 Hz), middle frequency (20 Hz) and high frequency (50 Hz) of the seismic bandwidth. The outputs from the selected frequencies were combined into a single RGB blended full-colour image, and this result enables the analysis of different channel features. Our experiment using the S-transform algorithm was conducted on the seismic data of time slice 230 ms.

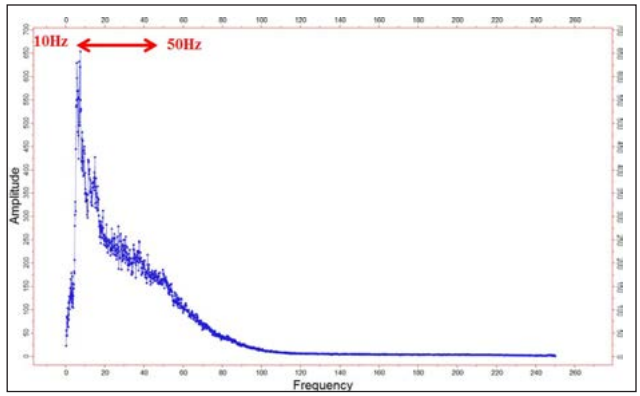

Figure 3: Graph showing Frequency versus Amplitude of the seismic data.

When the original amplitude (Figure 4a) was compared to the output from the spectral decomposition (Figure 4b), the result from the spectral decomposition exhibits channel system that existed at maximum prominence in time slice 230 ms. Where the shape of the channel becomes increasingly visible (green circle loop), prediction of actual volume and size of the channel (white and red circle loop) and type of channel can be deciphered (blue circle loop). Figure 4b shows the seismic geomorphology from using spectral decomposition, which has allowed better delineation and, has distinguished the type of channels features by their size and width; such as point bar, flood plain, meandering channel, thalweg, straight channel and anastomosing channel that existed in the N-Field area (Figure 4). At the optimum frequency, the result shows the increase in the volume of tributaries channel features, identified in the direction of S-W in the map. The white patches are the thinnest parts of the channel (present from a combination of selected frequencies range).

Referring to Ethridge & Schumm (2007), the channel patterns and characteristic of lithology classification is based on the degree and character of sinuosity. In general, high sinuosity channel is mainly sand filled, and low sinuosity channel is either shale or sand-filled. Low sinuosity channel is in the southern part of the study area, which constitutes a tributary channel that formed during the sea-level lowstand. The high sinuosity channel is in the upper part of the area, i.e., differentiated by small and medium scale. The meandering channels are attached to point bar deposits. These point bars are known by the high amplitude, i.e., they are associated with very well developed meander scrolls. The meandering

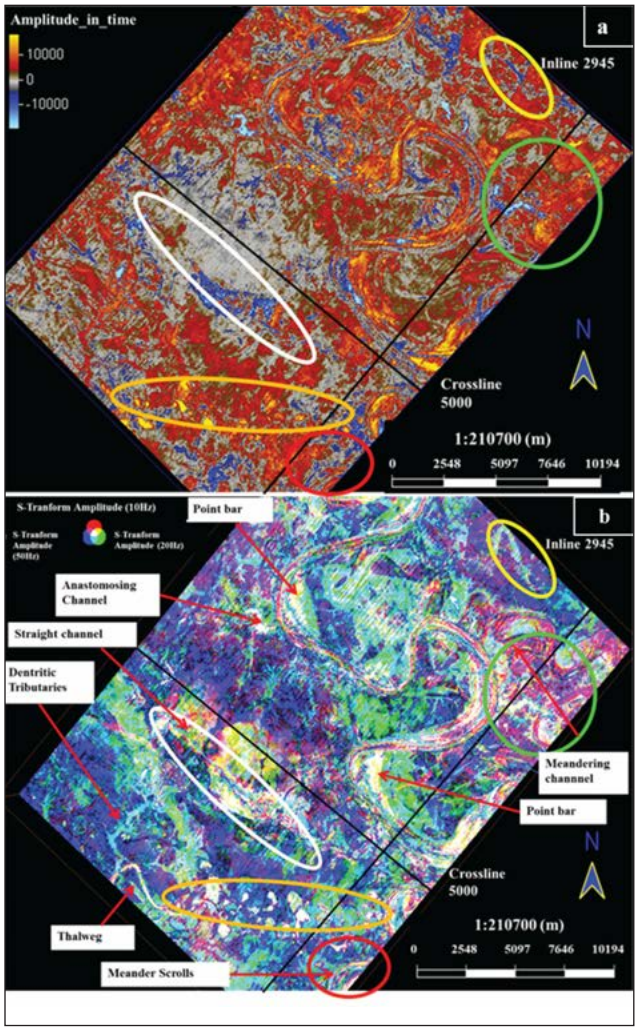

Figure 4: (a) Original amplitude, (b) applying spectral decomposition with low frequency (10Hz), middle frequency (20Hz), and high frequency (50Hz) revealed geomorphological patterns that reflect different tuning thickness.

rivers scroll flowed most of the eastward towards the study area in the association, i.e., the larger meandering channels were imaged The meandering channel is highly sinuosity towards the northeast direction. A neck cutoff abandoned channel (Figure 4b) is noticeably imaged in the downstream part of the channel as suggested by Schumm (2005), which a continued sea-level rise have caused the channel to decrease its sinuosity, while the meandering channels linked up with point bars and are interpreted to have developed during the main transgressive period. The channel system in time slice 530 ms showed in Figure 5 is also affected by faults that appear to be post-development of the channel. Channel formation started to exist in time slice 2606 ms till 230 ms to recent. Based on the formation of the interest (i.e., Group E to Group A and B) that was deposited during Late Miocene to Recent, the formation contains the biggest channel network from braided to meandering channel system. Most of the channels recorded in Pleistocene age are features of an incised valley which demostrate a regular depositional environment. It indicated an area with rapid modifications in sea level that forms transgression sequences. The meandering rivers were associated with point bars and are interpreted to have developed during the main transgressive or sea-level rise period (Late Pleistocene time). These meandering channels have different sizes and are of varying sinuosity. These differences could be caused by the type of sediment load and the discharges (Schumm, 2005).

Ant tracking attribute

Ant tracking attribute is useful to describe fault characteristics and is also an excellent attribute for tracking the discontinuity of reflector in seismic data. The ant tracking algorithm was developed based on the ant territory system to interpret discontinuity structure in noisy data. This attribute uses the principle of swarm intelligence. As mentioned by Pederson *et al.* (2002), swarm intelligence is practised

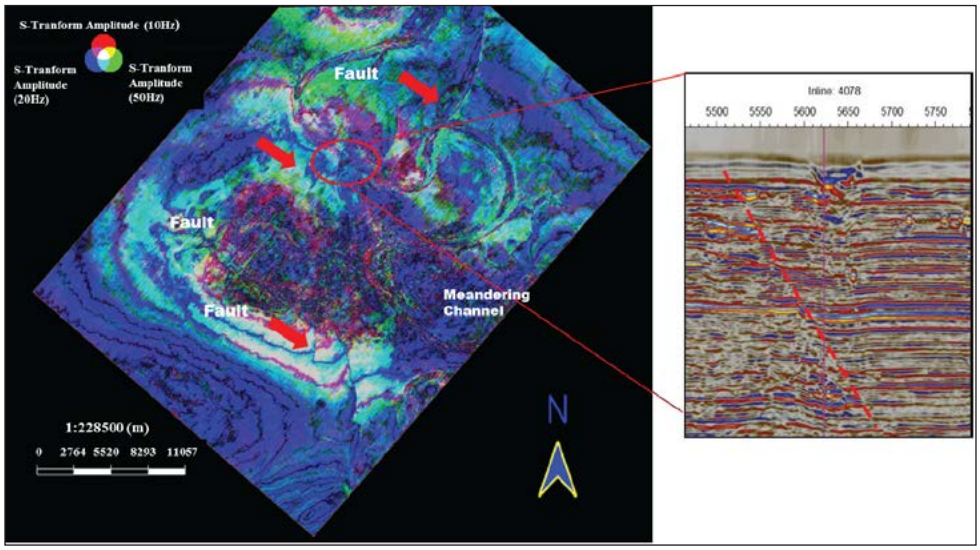

Figure 5: Shows time slice 530 ms faults bounded with the channel with evidence given in Inline 4078.

to determine, track and sharpen faults, which mimics the collective behaviour of social ants in nature in finding the shortest path between their nests and food source, by interacting with each other using chemical substances known as phenomenon. In searching for food, ants use phenomenon trails to direct other colony members to the food source they have found. Similar to this concept, virtual ants are put as a seed on a seismic discontinuity volume to search or detect fault zones, which, by this way, the virtual phenomenon positioned by the ants interprets information related to the fault zones in the volume (Celine *et al.,* 2005). It is to be noted that the discontinuity attribute will not only detect a fault in a seismic data, but will also enhance other discontinuities such as channel boundaries, noise, and chaotic response. With ant tracking algorithm, non-structural features such as noise and channel will be less noticeable due to their intermittent internal chaotic textures that stops the ant tracker from extricating these non-surface shaped features (Jansen, 2005).

The workflow of ant tracking algorithm consists of 4 compulsory paths, which are seismic data conditioning, edge detection and enhancement and fault surface extraction. In general, the ant tracking workflow preprocessing will involve structural smoothing, filtering options, followed by discontinuing attributes such as chaos or variance (Table 1). In this study, the structural smoothing method is used as the main input signal guided by the local structural to boost the continuity of the seismic reflectors. The ant tracking algorithm is practised with several main steps:

- Seismic conditioning - upgrading of the seismic data volume by applying a spatial filter to diminish background noise and to aid the spatial continuities of a seismic signal.
- Edge detection - finding the true edge by tracking the algorithms.
- Edge enhancement - two attributes were extracted (variance and chaos).
- Surface extraction - generation of faults surface.

There are several ant tracking parameters, including the initial ant boundary, ant track deviation, ant step size, illegal steps allowed, legal steps required and stop criteria (Table 2). The initial ant boundary is assigned to control how closely the initial ant agents can be placed within the volume, and this distance is measured in terms of voxels and is the primary control for the number of agents generated. Ant track deviation allows the ants to search a larger number of voxels on either side of their tracking direction, where a large value will allow more connections between ant agents. The 'step size' commonly used is size three, which refers to how far an ant can advance for each increment of its search. Increasing this value allows the ant to search further, finding more connections but at a larger resolution. When the ant tracking fails to continue edges, it will be allowed to advance further by three parameters: the illegal steps allowed, legal steps required and stop criteria. The illegal steps required working together with the illegal step parameter by demanding the selected number of valid steps after an illegal step.

The parameter of stop criteria also acts in combination with the illegal steps and is utilised to dismiss the ant's progress when excessive illegal steps have been made. In this paper, the differences between the parameters are tested, and the best parameter is selected for each different attributes.

By applying structural smoothing (Figure 6), the Gaussian Filter parameter shows good discontinuity and better visualisation. The structural smoothing was used in this study to enhance the seismic event continuity parallel to the estimated bedding orientation and to enhance the faults (Hameed *et al.,* 2017). Figure 6a shows the original seismic amplitude, and Figure 6b shows the seismic amplitude with application of the structural smoothing which shows good resolution and continuity of the seismic events. The

Table 1: Parameters used in conditioning the seismic volume.

Structural Smoothing	Filter option Plain	Sigma X 1.5	Sigma Y 1.5	Sigma Z 1.5
Variance/ Chaos	Inline range 3	Crossline range 3	Vertical Smoothing 15	Dip Correction Off
3D Edge Enhancement	Horizontal/ Vertical radius 5/10	Plane half-thickness 0	Minimum/ Maximum dip 50/90	Minimum/ Maximum Strike 0/180

Table 2: Ant tracking parameters.

Initial Ant Boundary	Ant Track Deviation	Ant Step Size	Illegal Steps Allowed	Legal Steps Required	Stop Criteria
7	2	3	1	3	5

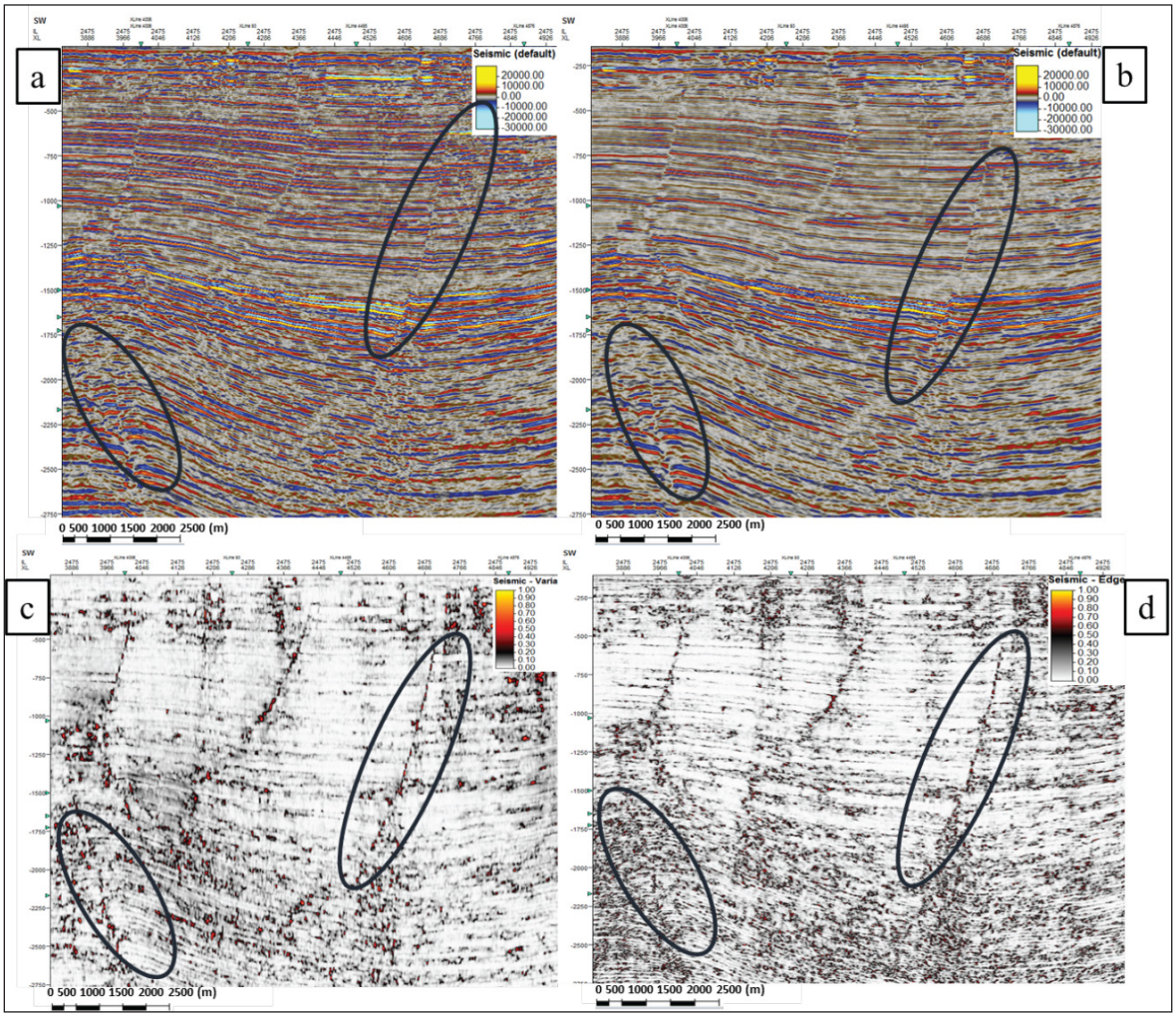

Figure 6: (a) Structural smoothing data applied without Gaussian Filter, (b) Structural smoothing data applied with Gaussian Filter, (c) Structure in the blue circular loop is seen in variance attribute, (d) Structure in the blue circular loop is seen in chaos attribute.

background noise effect has also been removed (Hameed *et al.,* 2017). The data set shown in Figures 6a and 6b (inline 2475) was used to generate the variance and chaos attributes. The variance and chaos attributes were used as input data to run the ant tracking attribute, as shown in Figure 7. As proof, a time slice map 1500 ms, Inline 2475 (dotted line), three Crossline representing green line (4606), red line (4406), and blue line (4006) are shown in Figure 7. The major faults are not clearly seen in the amplitude data since the area have been breached due to presence of gas chimney, however, chaos (Figure 7a) and variance (Figure 7b) attributes display the enhanced faults (discontinuities of seismic reflector). As shown by the green loop of the chaos attribute (Figure 7a), the major faults are clearly displayed here than when the variance attribute is applied (Figure 7b). Two comparison maps of fault lineament trend are justified in Figure 7c to validate the fault interpretation by ant tracking algorithm. The maps, i.e., surface map and ant tracking surface map shows fault lineament and has led to recognition of present N-Field faults. The faults were identified by looking at the faults planes separated by the fault throw block positioned along its plane. As a final result for fault interpretation, a total of 37 fault segments were interpreted within N-Field by ant tracking attribute. The identified faults strike along the southwest-northeast direction and are steeply dipping towards the west and east (Figure 8) in Inline 2615. Based on the interpretation, en echelon patterns due to wrench movements are present in the area. Wrench motion created en enchelon fault patterns and pull-apart the area to the right continuosly as shown in Figure 8. Later wrench motion caused inversion and drag folds may occurred. Compression forces with the principle of the forces direction at the maximum σ1 of relatively trending Northeast to Southwest causing the rock in the N-Field to be deformed with minor folds to form drag folds and normal faults. This give a clue that this area had been effected by compressional and tensional stress. This statement has been proven by Tjia (1998), referring to the structure of this area was inverted and indicated that the fault trending to the north and also left lateral changed formed

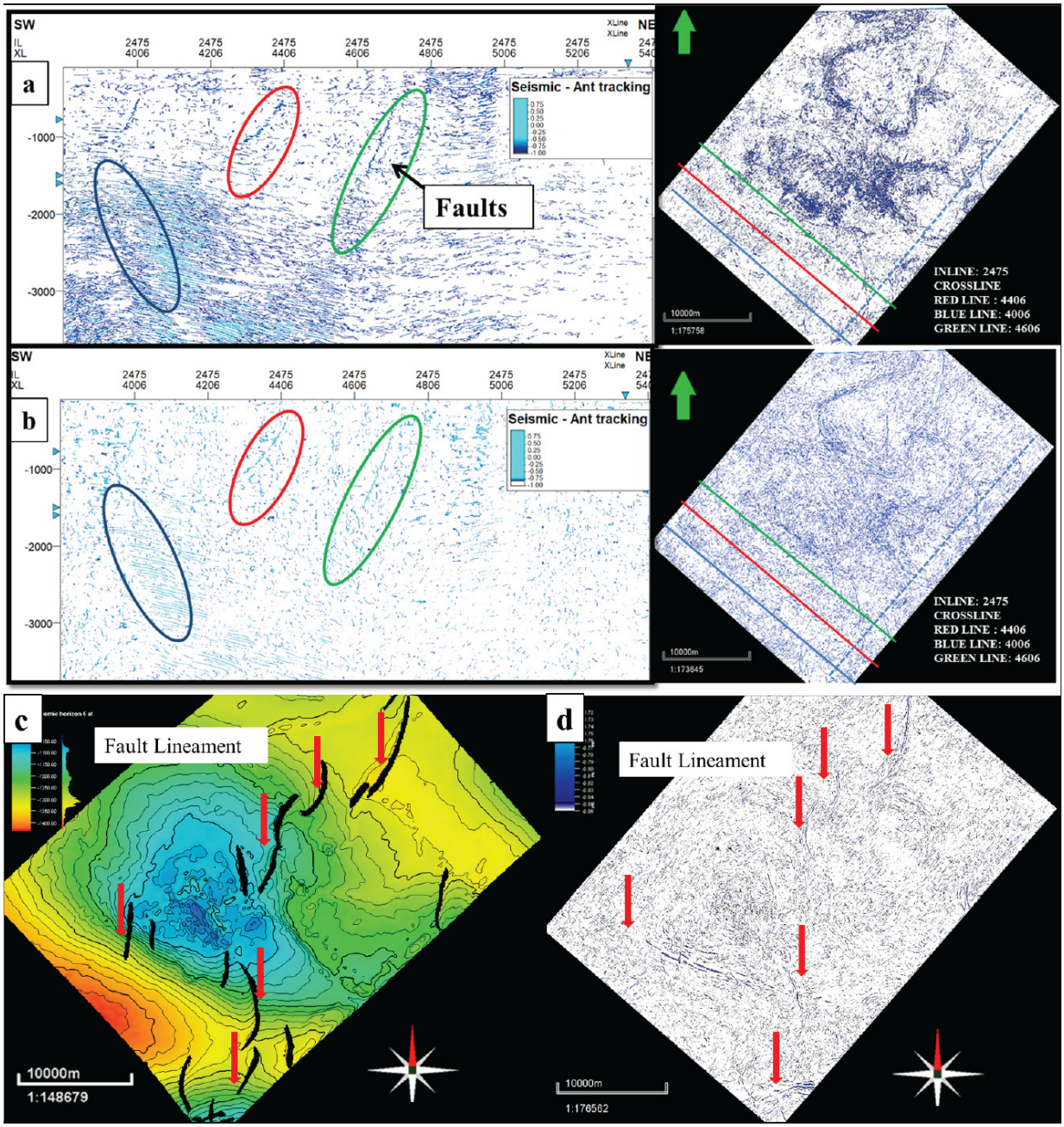

Figure 7: (a) Ant tracking using result with chaos attribute application, (b) ant tracking using result with variance attribute application, (c) fault lineaments shown in surface map, (d) fault lineaments shown in ant tracking map.

by revered slip movement. Anticlines are found above the half graben that suggested the structure went through an inversion phase. Most of the faults that has been interpreted have lengths ranging from 0.5 km to about 7 km. Based on the geobody interpretation (Figure 9), graben structure exists in the Southwest to Northeast part in the N-Field area, between Horizon 1 and Horizon 2. The lengths of the faults varies, but are less than 4 km.

The application of ant tracking algorithm is also useful to delineate more information about the gas cloud. Gas-cloud zones cause difficulty in translating the steadiness of the stratigraphic layering in these sections and is obtrusive for any structural deformation contained by the affected zone. The first view seismic data use the ant tracking is due to poor amplitude within the gas cloud zone. From ant-tracking algorithms, that work area structure is complex, the sizes of the gas cloud are intricate. However, ant tracking algorithms clearly can differentiate between sections affected by the gas cloud part and parts which are not influenced by the gas cloud zone. The details of small fractures due to the structure of gas cloud have been demonstrated, i.e., reflected on a single ant tracking

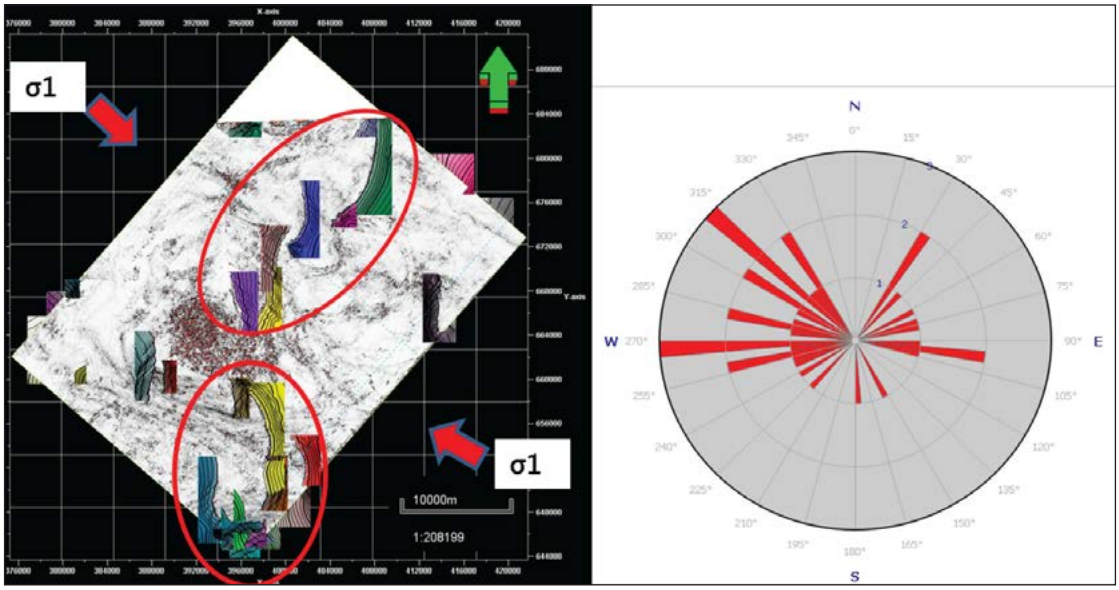

Figure 8: Fault trends and principle of the direction of the forces at the maximum σ1 along the Southwest-Northeast direction and steeply dipping towards the west and east.

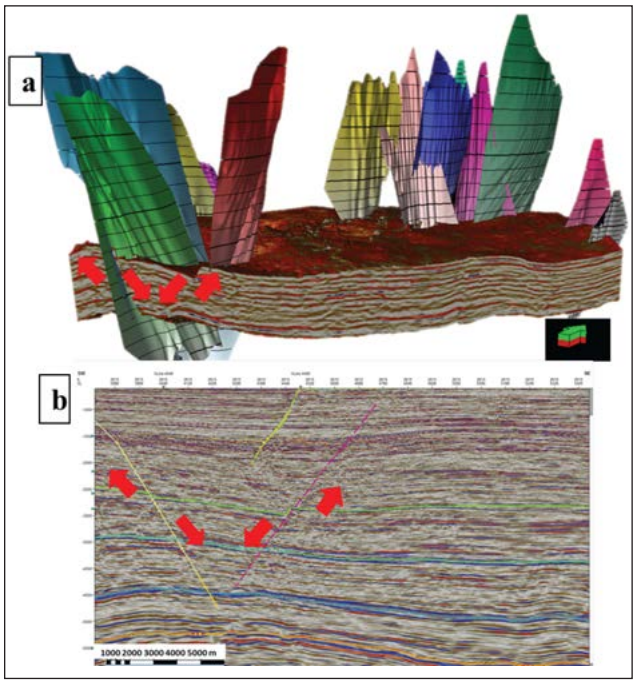

Figure 9: (a) Geobody of Horizon 1 and Horizon 2 bounded with faults surface, (b) existance of graben in Inline 2615.

body. Tone shaded of ant tracking marks high fracture, and high anomalies relationship is clearly affected by gas cloud zone, as shown in Figure 10a. While ant tracking marks of low fractures and low anomalies are the parts not affected by gas cloud. The gas cloud on ant tracking colour changes significantly; the ant tracking trace colour about the reliable gas cloud of large size is significantly darker than the less reliable.

The ant track time slice -80 ms displayed in chaos ant track body clearly recognised the effect that shows the pockmarks characteristics (Figure 10b). As proven, acoustic blanking happens in Inline 4080 is showing the vertical seismic wipeout zone. According to Jamaludin *et al*. (2015), acoustic blanking happens when some seismic data is missing. It shows the patterns in a seismic wiped out zone because seismic wave effects show from bad reflector and dissipation. The existence of pockmarks is also an indicator concerning the existence and formation of faults that have happened.

CONCLUSION

In this paper, the application of spectral decomposition by using S-transform method on the seismic data can reveal geological information in the time and frequency domain. The result shows that spectral decomposition is an effective tool for revealing volume, allowing better delineation and provides specific type of channel features according to its size and width. Spectral decomposition can be utilised to discover thinner channels within the a wider channel and thus, that leads to the expectation of lithology sand distribution, preservation of abandonment channel and development of scrolls. Spectral decomposition demonstrates the way bed thickness can be recognised by dissimilar frequency wavelets and their correlation between thin beds tuning within a channel. Part of the channel that was run via lower frequency captures the thicker beds compared to the higher frequency, which apprehends the thinner beds. Channels were classified into high sinuosity (Southern) and low sinuosity channels (Northeast). These highlights the important role that sediment in meandering channel systems may have on stratigraphic trap development. In addition to sea-level

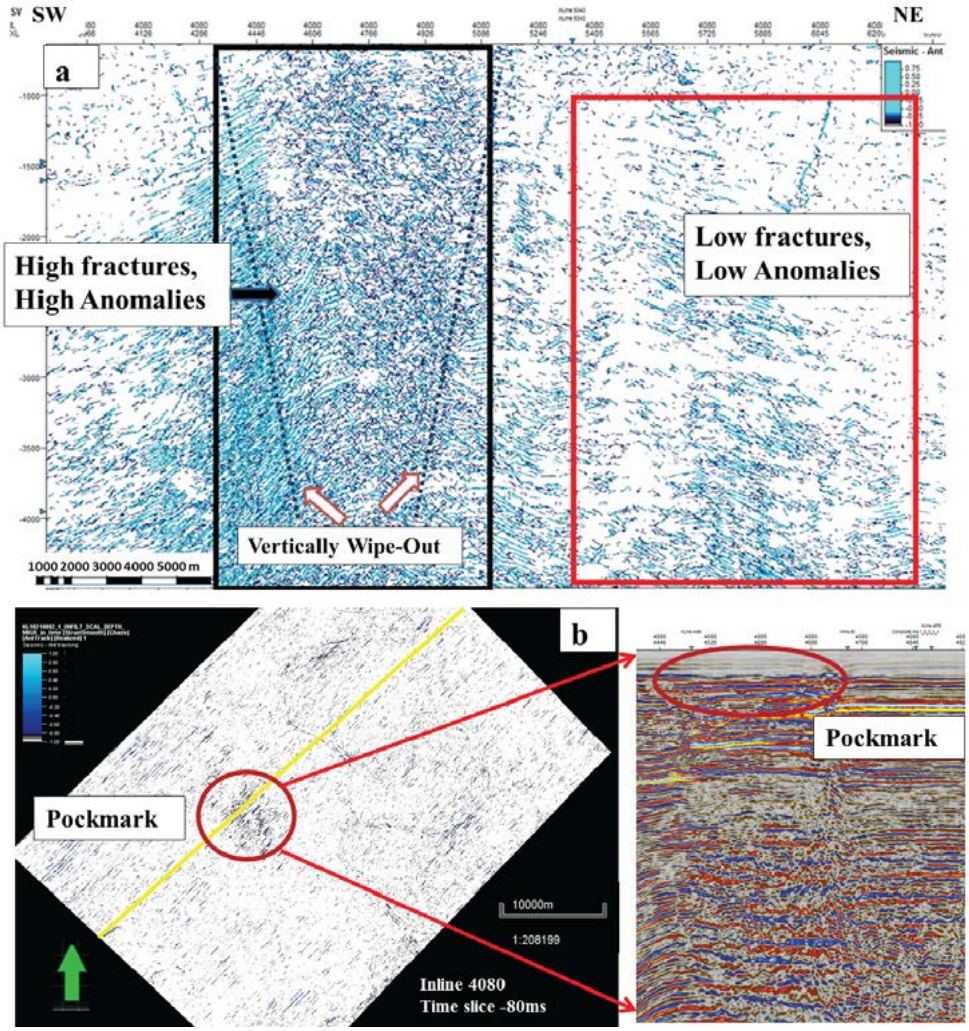

Figure 10: (a) The black box shows area which has high fractures and high anomalies relationship that is clearly affected by gas cloud zone, and red box shows area of low fractures and low anomalies which is not affected by gas cloud in the section inline 4080 by ant tracking algorithm, (b) the section time slice 80 ms shows existence of pockmarks.

changes, the observed difference in the size of the channel may be related to varying discharge, which in turn may be related to climatic variations. For structural interpretation, the results indicated that ant tracking is a decent practice for improving faults. One of the appropriate usage of filtering is to enhance the signal and noise ratio without smearing faults, since seismic attributes are sensitive to noise. The variance and chaos attributes using ant tracking give good results and can show more lineaments (fracture) due to gas dissipation. Result of fault interpretation leads to the initial understanding of fault systems with automatically extracted surfaces, and the interpreter starts with a structural summary of the faults in the area. Therefore, from the start, the interpreter will be analysing in terms of the fault system and tectonic history of the area.

ACKNOWLEDGEMENTS

Firstly, the authors wish to thank Universiti Teknologi PETRONAS (UTP) and the Centre of Seismic Imaging (CSI) for providing the facilities, and PETRONAS for research data and permission to publish. Thank you to all my friends for their ideas and contributions. Finally, we thank the reviewers for their constructive comments which helped to improve the quality of the manuscript.

AUTHOR CONTRIBUTIONS

NSS conceptualized, computed, analysed, interpreted results (structural and stratigraphy interpretation) and wrote the paper. NA, ME and DPG analysed, interpreted results and helped to draft the manuscript. All authors reviewed the results and approved the final manuscript.

CONFLICT OF INTEREST

The authors have no conflicts of interest to declare that are relevant to the content of this article.

REFERENCES

Bishop, M. G., 2002. Petroleum System of the Malay Basin Province, Malaysia. Reston, VA, 21 p.

Celine C. S., Cristiano S. M. & Fabrizio D. L., 2005. Automatic Fault Extraction Using Ant Tracking Algorithm in the Marlim South Field, Campos Basin. SEG Technical Program Expanded Abstract, 857–861.

Chopra, S. & Marfurt, K. J., 2007a. Volumetric curvature attributes adding value to 3D seismic data interpretation. Society of Exploration Geophysicists - 77th SEG International Exposition and Annual Meeting, SEG 2007, (2002), 851–855.

Chopra, S. & Marfurt, K. J., 2007b. Seismic attributes for prospect identification and reservoir characterisation. Geophysical Development Series No. 11 (SEG Geophy.). Society of Exploration Geophysicists, Tulsa USA. 481 p.

Ethridge, F. G. & Schumm, S. A., 2007. Fluvial seismic geomorphology: A view from the surface. Geological Society Special Publication, 277, 205–222.

Ghosh, D., Halim, M. F. A., Brewer, M., Viratno, B. & Darman, N., 2010. Geophysical issues and challenges in Malay and adjacent basins from an E & P perspective. The Leading Edge, 29(4), 436-449.

Ghosh, D., Sajid, M., Ibrahim, N. A. & Viratno, B., 2014. Seismic attributes add a new dimension to prospect evaluation and geomorphology offshore Malaysia. The Leading Edge, 33(5), 536–545.

Hutchison, C. S., 2014. Tectonic evolution of Southeast Asia. Bulletin of the Geological Society of Malaysia, 60, 1-18.

Huang, Z. L., Zhang, J., Zhao, T. H. & Sun, Y., 2016. Synchrosqueezing S-Transform and Its Application in Seismic Spectral Decomposition. IEEE Transactions on Geoscience and Remote Sensing, 54(2), 817–825.

Hameed, E.R.N.A., Ali Bakr, A.M. & Dahroug, S. M., 2017. Seismic data interpretation for hydrocarbon potential, for Safwa/Sabbar field, East Ghazalat onshore area, Abu Gharadig basin, Western Desert, Egypt. NRIAG Journal of Astronomy and Geophysics, 6(2), 287–299.

Jansen, K., 2005. Seismic investigation of wrench faulting and fracturing at Rulison Field, Colorado (Doctoral dissertation, Colorado School of Mines).

Jamaludin, S. N. F., Abdul Halim Abdul Latiff & A.Kadir, A., 2015. Interpretation of Gas Seepage on Seismic Data: Example from Malaysian offshore. IOP Conference Series: Earth and Environment Science, 30(012002), 660 p.

Kuyuk, H. S., 2015. On the use of Stockwell transform in structural dynamic analysis. Sadhana - Academy Proceedings in Engineering Sciences, 40(1), 295–306.

Liew, K. K., 1997. Structural analysis of the Malay Basin. Bulletin of the Geological Society of Malaysia, 40, 157–176.

Metcalfe, I., 1988. Origin and assembly of south-east Asian continental terranes. Geological Society London Special Publications, 37(1), 101–118.

Madon, M., Abolins, P., Hoesni, M. J. & Ahmad, M., 1999. Malay Basin. The Petroleum Geology and Resources of Malaysia, Kuala Lumpur, 171-217.

Martins, J. F., Lopes, R., Fernao Pires, V., Pires, A. J. & Lima, C., 2012. The application of S-transform in fault detection and diagnosis of grid-connected power inverters. IECON Proceedings (Industrial Electronics Conference), 5247–5252.

Mansor, M. Y., Rahman, A. H. A., Menier, D. & Pubellier, M., 2014. Structural evolution of Malay Basin, its link to Sunda Block tectonics. Marine and Petroleum Geology, 58(PB), 736–748.

Ngah, K., 2000. Structural framework of Southeastern Malay Basin. Search and Discovery Article #10009(2000), 1–21.

Nanda, N. C., 2016. Analysing Seismic Attributes. In: Nanda N.C. (Ed.), Seismic Data Interpretation and Evaluation for Hydrocarbon Exploration and Production. Springer, Cham, 171–185.

Pedersen, S. I., Randen, T., Sonneland, L. & Steen, O., 2002. Automatic 3D Fault Interpretation by Artificial Ants. 64th EAGE Conference & Exhibition, 512-515.

Petronas. (n.d.). Appraisal well.

Schumm, S. A., 2005. River Variability and Complexity. Cambridge University Press, New York. 220 p.

Stockwell, R. G., 2007. Why use the S-transform. Pseudo-differential operators: partial differential equations and time-frequency analysis. Fields Institute Communications Series, 52, 279–309.

Tjia, H. D., 1998. Origin and tectonic development of Malay-Penyu-West Natuna basins. Bulletin of the Geological Society of Malaysia, 42(42), 147–160.

Manuscript received 19 June 2020;
Received in revised form 26 October 2020;
Accepted 30 November 2020
Available online 16 November 2021